Polarization-difference imaging: a biologically inspired technique for observation through scattering media

M. P. Rowe and E. N. Pugh, Jr.

Institute of Neurological Sciences, University of Pennsylvania, Philadelphia, Pennsylvania 19104

J. S. Tyo and N. Engheta

Moore School of Electrical Engineering, University of Pennsylvania, Philadelphia, Pennsylvania 19104

Received August 17, 1994

Many animals have visual systems that exploit the polarization of light, and some of these systems are thought to compute difference signals in parallel from arrays of photoreceptors optimally tuned to orthogonal polarizations. We hypothesize that such polarization–difference systems can improve the visibility of objects in scattering media by serving as common-mode rejection amplifiers that reduce the effects of background scattering and amplify the signal from targets whose polarization-difference magnitude is distinct from the background. We present experimental results obtained with a target in a highly scattering medium, demonstrating that a manmade polarization-difference system can render readily visible surface features invisible to conventional imaging.

Optical scattering by suspended particles (e.g., fog, rain, plankton) diminishes the visual contrast of objects.[1–3] Although polarization-sensitive vision is well documented as serving in navigation,[1,4,5] some types of polarization-sensitive vision also may serve to enhance the visibility of targets in scattering media.[6,7] The goal of this Letter is to demonstrate that a manmade polarization-difference imaging (PDI) system, similar to that hypothesized to function in some biological visual systems,[7,8] can enhance the visibility of target features in a scattering medium.

Our PDI system captures images of a scene at two orthogonal linear polarizations, computes the difference of the images pixel by pixel, and rescales the resultant difference image for optimum use of the monochrome display range. Symbolizing the two image intensity distributions as $I_{\parallel}(x,y)$ and $I_{\perp}(x,y)$, where (x,y) identifies the pixel position in the image and $\parallel$ and $\perp$ indicate two orthogonal linear polarizations, the PDI system generates the polarization-difference (PD) and polarization-sum (PS) images:

$$_{\mathrm{PD}}I(x,y) = I_{\parallel}(x,y) - I_{\perp}(x,y)\,, \qquad (1a)$$

$$_{\mathrm{PS}}I(x,y) = I_{\parallel}(x,y) + I_{\perp}(x,y)\,. \qquad (1b)$$

If an ideal linear polarizer is used to measure $I_{\parallel}$ and $I_{\perp}$, then the PS image is equivalent to a polarization-blind image obtained by a conventional imaging system. In general, $_{\mathrm{PD}}I$ depends on the choice of polarization axes, whereas $_{\mathrm{PS}}I$ does not. The choice of the orthogonal axes will be discussed shortly.

The experimental layout is shown in Fig. 1. Two incandescent tungsten filament slide projectors backilluminate a sheet of 0.64-cm-thick white Plexiglas attached to a glass tank. The tank is filled with water to which milk is added. The Plexiglas acts as an initial diffuser and the milk as a strong scattering agent. The tank is viewed with a CCD camera (Hamamatsu Model XC-77) equipped with a macro lens (Vivitar Y/C 55 mm, f2.8). Images are digitized and processed by an image analysis system that has a 16-bit frame buffer (accumulator) (Imaging Technology Series 151). In the absence of a target, the region viewed by the camera has an average apparent radiance of ~7.2 W/(m^2 sr) uniform to within 15%, and its light is essentially unpolarized. The target is an aluminum disk suspended in the middle of the tank by means of a rod attached to the back face of the disk, i.e., the face hidden from the camera. The end of the rod not attached to the target disk is inserted into a clear Plexiglas mount suspended from above; the surface of this mount is perpendicular to the incident light, and both it and the rod are completely invisible to both PDI and conventional imaging. Except for two 1-cm^2 patches, the disk surface facing the camera is

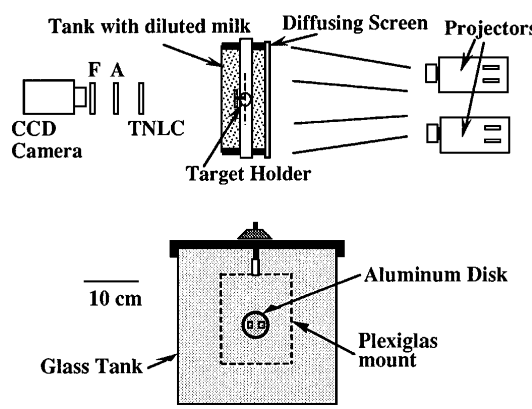

Fig. 1. Top: the top view of the experimental setup. A, polarization analyzer; TNLC, twisted nematic liquid crystal; F, narrow-band filter. Bottom: the front view of the tank (drawn to scale) with inside dimensions of 30 cm × 30 cm × 15 cm. This tank is filled with water to which 5 mL of whole milk is added. The measured beam attenuation coefficient for a 632.8-nm laser beam is 19.7 m^{-1}. Thus the tank depth is ~2.9 attenuation lengths at this milk concentration. The sensitivity of the imaging system at 610 nm is ~4.4 × 10^{-7} display units/(quanta s^{-1}) (in 8-bit display).

0146-9592/95/060608-03$6.00/0 © 1995 Optical Society of America

sandblasted, rendering it nearly Lambertian. These patches, whose relative locations are shown in Fig. 1, are a few thousandths of an inch higher than the sandblasted background and have been abraded with emory paper lightly in orthogonal directions—on one patch vertically, and on the other horizontally. The image-forming light from the target surface results from multiple scattering: photons scatter off milk particles to the target surface, and some of these are scattered again toward the camera. Before reaching the camera, the light from the tank passes through a twisted nematic liquid crystal (TNLC; Liquid Crystal Institute, Kent State University.) In its off state, the TNLC rotates the plane of polarization of incident light by 90°; when driven, the TNLC passes the incident light with no rotation. After the TNLC, the light passes through a linear polarization analyzer. A narrow-band filter (10 nm FWHM, centered at 610 nm) eliminates light outside the operating waveband of the TNLC. When the TNLC is driven, the TNLC/analyzer passes only light polarized *parallel* to the analyzer axis, yielding the image $I_{\parallel}$; when the TNLC is off, the TNLC/analyzer combination passes light polarized *perpendicular* to the analyzer axis, yielding $I_{\perp}$. For the results reported here, the analyzer axis was oriented vertically.

Figure 2 illustrates the application of the PDI system to the imaging of the aluminum target suspended in diluted milk. Figures 2A and 2B present the images, $I_{\parallel}$ and $I_{\perp}$, convolved with a two-dimensional (low-pass) filter. To generate Figs. 2A and 2B, we summed 128 consecutive 33-ms frames and then divided by 8. Figures 2C and 2D present ${}_{\rm PS}I$ and ${}_{\rm PD}I$, respectively, the sum and difference images. Figures 2E and 2F re-present the data in images in Figs. 2C and 2D transformed with affine transformations to use the full intensity range of the display. The abraded patches, which are not visible in Figs. 2A–2D, are clearly visible in the transformed PD image (Fig. 2F) but practically invisible in the transformed PS image (Fig. 2E). Figures 2A′–2F′ present numerical plots of average pixel intensities in the pixel region $y_1 \leq y \leq y_2$, as illustrated by the arrows shown in Figs. 2B, 2D, and 2F; these plots provide quantitative evidence that supports the qualitative conclusion drawn from inspection of the images.

The principal factor underlying the enhanced visibility of the two patches in Panel F is the

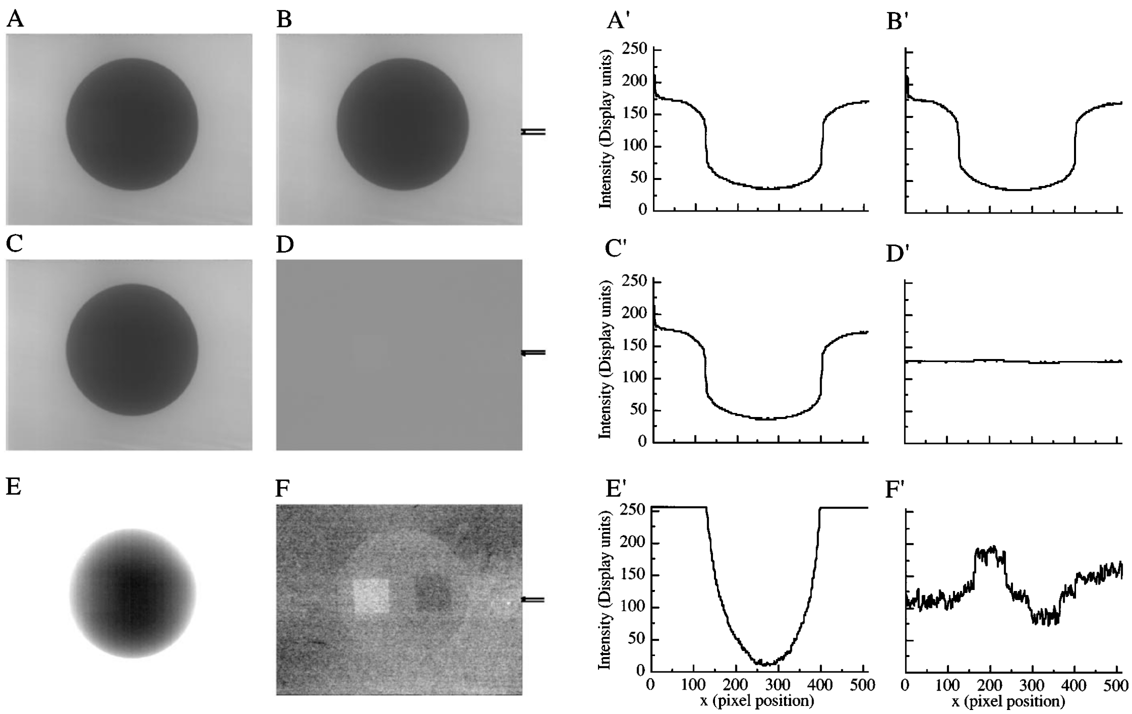

Fig. 2. Application of the PDI system to an aluminum target suspended in diluted milk as illustrated in Fig. 1. A, B, The images $I_{\parallel}(x, y)$ and $I_{\perp}(x, y)$ convolved digitally with a two-dimensional low-pass spatial filter. This filter is roughly a truncated Gaussian, with maximal linear extent ~5 pixel widths; the images of the abraded patches are ≈80 × 92 pixels. The filter removes a periodic high-spatial-frequency artifact produced by the imaging system. Image intensities (ordinates) are expressed in the units of the 8-bit display. C, D, ${}_{\rm PS}I(x, y)/2$ and ${}_{\rm PD}I(x, y) + 128$, respectively [cf. Eqs. (1a) and (1b)]; an offset of 128 was used, because most pixel values of ${}_{\rm PD}I(x, y)$ are near zero and can be positive or negative. E, F, The data of C and D, respectively, but transformed with affine transformations. The transformed values are given by ${}_{\rm PS}I(x, y)_{\rm trans} = \alpha_{\rm PS}[{}_{\rm PS}I(x, y) - {}_{\rm PS}I(x, y)_{\rm min}]$ and by ${}_{\rm PD}I(x, y)_{\rm trans} = \alpha_{\rm PD}[{}_{\rm PD}I(x, y) - {}_{\rm PD}I(x, y)_{\rm min}]$, where $\alpha_{\rm PS} = 255/[{}_{\rm PS}I(x, y)_{\rm max} - {}_{\rm PS}I(x, y)_{\rm min}]$, and similarly for $\alpha_{\rm PD}$. In E, ${}_{\rm PS}I(x, y)_{\rm max}$ and ${}_{\rm PS}I(x, y)_{\rm min}$ were obtained from the disk region only; the resultant scale factor, $\alpha_{\rm PS} \approx 6.4$, is such that the intensity variation of the disk region occupies the full display range. In F, ${}_{\rm PD}I(x, y)_{\rm max}$ and ${}_{\rm PD}I(x, y)_{\rm min}$ were obtained from the entire image, yielding $\alpha_{\rm PD} \approx 38.4$. Abraded patches, not visible in A–D, are clearly visible in F but practically invisible in E. The vertical bands of pixels in the pixel regions $y_1 \leq y \leq y_2$, as shown by the arrows at the right of panels B, D, and F, were averaged over y to generate numerical plots (as a function of x) shown in A′–F′.

common-mode rejection feature intrinsic to PDI. Given that a target feature may produce a nonzero value of ${}_{\mathrm{PD}}I$ in some region of the image, the system permits extraction of this feature by rejecting intensity common to both polarization axes. This common-mode rejection feature of the PDI system is exhibited in two ways in the images of Fig. 2. First, the relatively intense halo of unpolarized light surrounding the disk is eliminated from the PD image (cf. Figs. 2C′ and 2D′). Second, the effect of the relatively modest variation (~20% of total display range) across the disk surface is also minimized. This modest intensity variation masks the visibility of the target features in the PS image, and its rejection allows a higher gain to be applied to the PD image than to the PS image (cf. Figs. 2E′ and 2F′).

On the basis of the results shown in Fig. 2 and other data we have obtained, PDI has a general applicability. First, PDI is quite sensitive to intrinsically small signals. For a particular region of an image, the observed degree of linear polarization (ODLP), defined as $\langle \mathrm{ODLP} \rangle_{\mathrm{region}} = \langle {}_{\mathrm{PD}}I(x, y) \rangle_{\mathrm{region}} / \langle {}_{\mathrm{PS}}I(x, y) \rangle_{\mathrm{region}}$, serves as a dimensionless measure of the PD signal magnitude. For the left patch, $\langle \mathrm{ODLP} \rangle = +0.0164$; for the right patch, $\langle \mathrm{ODLP} \rangle = -0.0138$. Moreover, in experiments in which we have systematically raised the milk concentration to degrade the images until the target patches are undetectable, target patches having $\langle \mathrm{ODLP} \rangle \lesssim 0.01$ still could be readily seen on inspection of the PD image (data not shown). The images of many object surfaces in natural environments predictably will have ODLP's of considerably higher magnitude.[9] Second, PDI can be generalized readily to scattering environments in which the background itself has nonzero ${}_{\mathrm{PD}}I(x, y)$ for a given set of orthogonal polarization axes. Judicious orientation of the analyzer in the PDI system can enhance the ${}_{\mathrm{PD}}I$ of target regions relative to that of the background in the image plane.[10] Finally, PDI possesses the generally useful qualities of being passive, simple, and potentially very fast. PDI can operate passively in any region of the electromagnetic spectrum in which natural radiation exists. PDI is simple, in that it does not require the use of sophisticated image processing techniques; nevertheless, any image processing techniques can be added to, or used in parallel with, PDI to make it even more effective. PDI is also potentially very fast. In our current setup, it takes 4–5 s to obtain each of $I_{\parallel}$ and $I_{\perp}$, but this rate limitation is imposed by the low light levels achievable with monochromatic light and by the frame rate (30 Hz) and limited sensitivity of our imaging system. With a more-sophisticated system, a higher speed could be achieved with a successive-frame differencing technique. Furthermore, PDI also can be made very much faster by implementation in a massively parallel system, as nature appears to have done in the retinas of many animals.[7,8]

Other optical imaging techniques also employ polarization information.[3,11–17] However, in some of this work, the state of polarization of the illuminating light has been known and is typically under the experimenters' control.[3,11,12] In contrast, in PDI the light incident on the target does not have to be polarized, nor need its state of polarization be known or under the control of the imaging system. In other related work[13–17] in which there is no control over the polarization of illuminating light either the Stokes parameters have been mapped onto colorimetric coordinates[13,17] or ${}_{\mathrm{PD}}I(x, y)/{}_{\mathrm{PS}}I(x, y)$[14–16] or some form of percent polarization and polarization angle[16,17] has been mapped onto the z axis of a monochrome display. Mapping ${}_{\mathrm{PD}}I(x, y)/{}_{\mathrm{PS}}I(x, y)$ onto intensity confounds the common mode with the signal. In contrast, our technique removes the common mode and allows us to maximize the display of information that survives the common-mode rejection. The variation and magnitude of ${}_{\mathrm{PD}}I$ are usually less than the variation and magnitude of ${}_{\mathrm{PS}}I$ across the scene. Thus, to use the full dynamic range of a display, higher amplification can be applied to ${}_{\mathrm{PD}}I$ and thus some of the target features not visible to polarization-blind imaging can be observed with PDI.

This work is supported by U.S. Department of the Navy Office of Naval Research grant N00014-93-1-0935 and, in part, by the University of Pennsylvania Research Foundation.

References

1. J. N. Lythgoe, *The Ecology of Vision* (Oxford U. Press, London, 1979), pp. 112–127.
2. S. Q. Duntley, J. Opt. Soc. Am. **53,** 214 (1963).
3. S. Q. Duntley, in *Optical Aspects of Oceanography,* N. G. Jerlov and E. Steemann Nielsen, eds. (Academic, New York, 1974), pp. 135–149.
4. K. von Frisch, Experientia **5,** 142 (1949).
5. T. H. Waterman, in *Vision in Invertebrates,* H. Autrum, ed., Vol. VII/6B of the Handbook of Sensory Physiology (Springer-Verlag, New York, 1981), pp. 281–469.
6. J. N. Lythgoe and C. C. Hemmings, Nature (London) **213,** 893 (1967).
7. D. A. Cameron and E. N. Pugh, Jr., Nature (London) **353,** 161 (1991).
8. M. P. Rowe, N. Engheta, S. S. Easter, Jr., and E. N. Pugh, Jr., J. Opt. Soc. Am. A **11,** 55 (1994).
9. G. P. Können, *Polarized Light in Nature* (Cambridge U. Press, London, 1985), pp. 74–99.
10. J. S. Tyo, University of Pennsylvania, Philadelphia, Pa. (undergraduate senior design project, 1994).
11. G. D. Gilbert and J. C. Pernicka, in *Underwater Photo-Optics, Seminar Proceedings* (Society of Photo-Optical Instrumentation Engineers, Bellingham, Wash., 1966), p. AIII-1.
12. B. A. Swartz and J. D. Cummings, Proc. Soc. Photo-Opt. Instrum. Eng. **1537,** 42 (1991).
13. J. E. Solomon, Appl. Opt., **20,** 1537 (1981).
14. G. F. J. Garlick, G. A. Steigmann, and W. E. Lamb, U.S. patent 3,992,571 (November 16, 1976).
15. W. G. Egan, W. R. Johnson, and V. S. Whitehead, Appl. Opt. **30,** 435 (1991).
16. J. Halajian and H. Hallock, in *Proceedings of 8th Symposium on Remote Sensing and Environment 1* (Environmental Research Institute of Michigan, Ann Arbor, Mich., 1972), p. 523.
17. R. Walraven, Proc. Soc. Photo-Opt. Instrum. Eng. **112,** 164 (1977).